Self-supporting smart air filters based on PZT/PVDF electrospun nanofiber composite membrane

Weidong He[1,2,3], Yinghe Guo[1,2,3], Yi-Bo Zhao[2,3], Fuze Jiang[2,3], Jean Schmitt[2,3], Yang Yue[2,3], Jingxian Liu[1,*], Junji Cao[4], Jing Wang[2,3,*]

[1]Filter Test Center, College of Resources and Civil Engineering, Northeastern University, NO. 3-11, Wenhua Road, Heping District, Shenyang, Liaoning 110819, China

[2]Institute of Environmental Engineering, ETH Zurich, 8093, Zurich, Switzerland

[3]Advanced Analytical Technologies, Empa, Ueberlandstrasse 129, 8600, Dübendorf, Switzerland

[4]Institute of Earth Environment, Chinese Academy of Sciences, No. 97, Yanxiang Road, Yanta Zone, Xian, Shanxi 710061, China

*Corresponding authors: jing.wang@ifu.baug.ethz.ch (J. Wang), 82003@126.com (J. Liu).

Abstract

Smart air filters are beneficial to provide highly efficient particle removal, treat multiple contaminants simultaneously and conserve energy during air filtration processes. Herein, a type of self-supporting smart air filter (SSSAF) was fabricated by sandwiching the VOC-responsive PZT/PVDF electrospun membrane with two metal mesh electrodes. Besides the high filtration efficiency for sub-micron particles, the SSSAF showed good responses to pressure drop in the range of 0 to 500 Pa via the electroactivity of PZT/PVDF membrane. In addition, the SSSAF achieved VOC sensing function via the swelling properties of PZT/PVDF membrane in organic vapors, demonstrated by its signal to 50 to 200 ppm ethanol gases. The SSSAF based nanogenerator was employed to harvest wind energy, which was further applied to inhibit bacterial growth without the need of additional power input. The results provide new insight into development of all-in-one smart air filters.

Key words

Self-supporting, smart air filter, sensors, energy harvesting, anti-bacteria

1. Introduction

Polymer fibrous air filters are widely used in hospitals, public and residential buildings and vehicles for air quality management [1,2,3]. Recent advances in polymer fibers spawn the smart air filters which have the potential benefits for providing highly efficient particle removal, treating multiple contaminants simultaneously and conserving energy. So far, various types of smart air filters have been developed, and each type generally possessed a single feature such as high filtration efficiency [4-6], sensing function [7-10] or antibacterial property [11,12].

High filtration efficiency is the basic requirement for smart air filters. It is well known that polymer fibrous air filters capture particles through mechanical filtration mechanisms including interception, inertia impaction and Brownian diffusion, as well as electrostatic mechanisms such as image and columbic forces [13-15]. Nano-fibres, possessing large surface area to weight ratios, are widely used in air filtration to provide improved filter efficiencies by enhancing mechanical filtration effects [16]. Recently, a smart self-powered triboelectric filter, capable of generating triboelectric charges to enhance the electrostatic filtration effect, was introduced for achieving high filtration efficiency [17-19].

The sensing function makes smart air filters “smart”. Pressure drop of the filter is often the most important parameter to be monitored in air filtration processes, because it can be used to indicate when to clean or replace the filter [8-10]. Volatile organic compounds (VOCs) are another important target for sensing. An additional catalytic system is usually equipped in the air filtration system to remove various VOCs. However, the energy consumption of non-stop heating the catalytic system to the reaction temperature all the time is very high [20]. Thus, the VOCs should be detected

to determine the heating time to minimize the energy cost. Monitoring parameters such as temperature, humidity and airflow rate which influence filter performance [21,22] is also desired. Currently, the measurement of the above mentioned parameters is mainly achieved by various sensors but not by the air filter itself. Several stimuli-responsive polymers, such as pH-responsive poly(4-vinylpyridine) [23], thermally sensitive poly(N-isopropylacrylamide) [24] and electroactive polyvinylidene fluoride (PVDF) [25], have been reported to be used as sensing materials. Fabricating smart air filters with stimuli-responsive polymers may realize the true "smart" of the smart air filters.

Another desired function of smart air filters is antibacterial property, because the microorganisms deposited on filters increase the risk of respiratory diseases [26]. By the addition of chitosan, silver nanoparticles, ZnO, or TiO_2, several types of antibacterial air filters were developed [12, 27-30]. However, the reported antibacterial air filters do not possess sensing function.

So far, a smart air filter with the combined properties of high filtration efficiency, sensing function and antibacterial property has not been reported. In this study, a self-supporting smart air filter (SSSAF) based on lead zirconate titanate (PZT)/PVDF electrospun nanofiber composite membrane was introduced. Thanks to the nanofiber structure, piezoelectric property and swelling effect in organic vapor of the PZT/PVDF membrane, the SSSAF demonstrated excellent performances in terms of filtration efficiency, VOCs and pressure drop sensing, and other functions including energy harvesting and bacterial inhibition. The results in this study provide new insights into developing smart air filters.

2. Experiments

2.1 Fabrication of self-supporting smart air filter (SSSAF)

2.1.1 Materials

Poly(vinylidene fluoride) (PVDF, average Mw ~ 180000, CAS number 24937-79-9) and N, N-dimethylformamide (DMF, anhydrous, 99.8 % CAS number 68-12-2) were purchased from Sigma-Aldrich. Acetone (⩾ 99.5%, CAS number 67-64-1) was obtained from VWR. Lead zirconate titanate (PZT, 99.9%) powder was purchased from QiJin New Material, China.

2.1.2 Fabrication and characterization of PZT/PVDF membrane

PVDF and PZT powder were dissolved in a mixture of DMF/acetone (1:1 wt.%), forming a 14 wt % PZT/PVDF solution. PZT was mixed with PVDF in weight ratios of 0 %, 0.5 %, 1 % and 2 %. A multi-jet electrospinning system (NaBond Technologies Co., Ltd.), consisting of three spinnerets and a rotating drum collector, was used for the fabrication of nanofiber membranes. A tip-to-collector distance of 10 cm, a solution flow rate of 1 mL/h and a voltage of 20 kV were applied. All PZT/PVDF membranes were dried in a vacuum oven at 70 °C for 24 h to fully evaporate the solvent. The morphology of the electrospun PZT/PVDF membrane was characterized by scanning electron microscopy (SEM, Quanta FEG 650). Image J software was utilized for analyzing the average diameter of nanofibers. The crystalline phase of the PZT/PVDF membrane was identified by X-ray diffraction (XRD, Bruker D8).

2.1.3 Fabricating VOCs sensor and pressure drop sensor on SSSAF

Fabrication of VOCs sensor. The PZT/PVDF membrane was cut into a round sample with an area of 100 cm^2. A square gold particle layer with an area of 1 mm^2 and a thickness of 40 nm was coated in the middle of the round PZT/PVDF sample by magnetron sputtering (Leica, EM ACE 600). As the VOCs sensing area, the two sides of this square were separately connected with wires to collect the response signal (Fig.

S1a).

The SSSAF itself is the pressure drop sensor. After fabrication of the VOCs sensor, the round PZT/PVDF membrane was sandwiched between two metal mesh electrodes which were connected with wires separately. The edge of the sandwiched PZT/PVDF membrane was sealed with a rubber ring, completing the pressure drop sensor (Fig. S1b). The two metal mesh electrodes have the mesh size of 2 × 2 mm and negligible pressure drop. Besides serving as electrodes for connecting the external test instruments and energy storage circuit, these two metal meshes were used to produce equal but opposite charges via the electrostatic induction of the piezo generated potential at the interface.

2.2 Piezoelectric characterization of SSSAFs

The piezoelectric voltage of the SSSAFs equipped with different PZT/PVDF membranes were evaluated by a test platform as shown in Fig. 1a. The SSSAF was clamped in a filter test chamber; a set of windmill blades driven by the air flow was set in front of the SSSAF to strike the filter to generate vibration. The piezoelectric signal generated by the vibration of SSSAF was recorded by a digital multimeter (Keithley, DMM 7510).

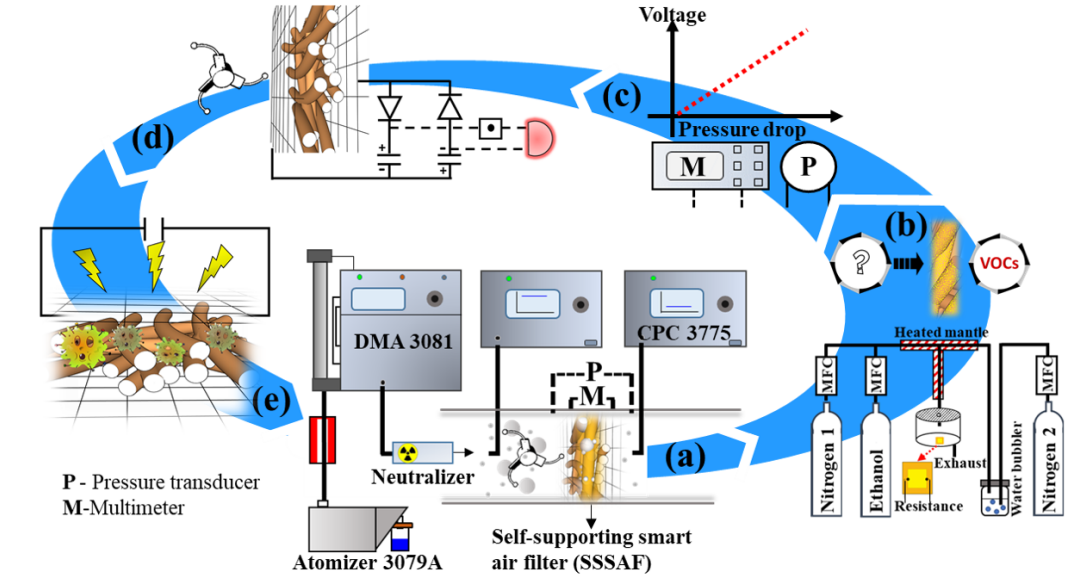

(a). Particle filtration test (b). VOCs sensing (c). Pressure drop sensing (d). Energy harvesting (e). Inhibiting bacteria

Fig. 1. The schematic diagram of SSSAF evaluation process for filtration efficiency, sensing functions and two special functions. a) Test of particle filtration efficiency. b) Test of VOCs sensing. c) Test of pressure drop sensing. d) Energy harvesting by the SSSAF based nanogenerator. e) Inhibiting bacteria by the harvested energy.

2.3 Particle filtration test for the SSSAF

The filtration efficiency of the SSSAF was measured by a test platform (Fig. 1a). Polydisperse NaCl aerosol was generated by an atomizer (TSI 3079A) and dried by a diffusion dryer. A differential mobility analyzer (DMA, TSI 3081) was used to select the particles with the target diameters. In this work, the particles with the mobility diameters of 50, 80, 100, 200, 300, 400, and 500 nm were selected. Two condensation particle counters (CPC, TSI 3775) were employed to measure the particle concentrations up- and down-stream, aiming to calculate the particle filtration efficiency of the filter. To understand the effects of the windmill blades on the filtration efficiency, the particle filtration test of the SSSAF was performed under both static (without the windmill blades striking the filter) and vibration conditions (with the windmill blades striking the filter). The face velocity of test was 5.3 cm/s.

2.4 Evaluation of the sensing functions of the SSSAF

2.4.1 Test of VOCs sensing

The resistive response of the VOCs sensor under controlled environment was characterized by using the setup shown in Fig. 1b. A water bubbler was used to control the relative humidity within 40%-60%, and the temperature was kept at 25 ℃ via a heated mantle.

Firstly, the SSSAF was installed in the gas test chamber sealed with Teflon tape, while the wires of the VOCs sensor were connected to the digital multimeter. Secondly, ethanol gases at different concentrations were prepared by diluting the pure ethanol gas with nitrogen, then the ethanol gas was fed into the gas test chamber at a constant flow rate of 10 ml/min. The sensor measurement consisted of exposure to the ethanol gas until the response signal stabilized and a subsequent purging with dry nitrogen to reset the baseline. The signal generated by dry nitrogen with equivalent flow rate of the ethanol gas was defined as the baseline for the sensor. Herein, the sensor responses were presented as the resistance difference between the response and baseline ($\Delta R = R_{response} - R_{baseline}$). The test concentrations of ethanol gas were in the range of 50 to 200 ppm.

2.4.2 Test of pressure drop sensing

On the basis of the filtration test platform shown in Fig. 1a, with the steps of particle selection by DMA and particle concentration measurement by CPC skipped, the polydisperse NaCl aerosol were directly loaded on the SSSAF after being dried and neutralized. The pressure drop of the SSSAF was measured by a pressure transducer (OMEGA PX409-10WDWUUSBH) during particles loading, and the piezoelectric voltage signals corresponding to the growth in pressure drop of 0, 100, 200, 300, 400

and 500 Pa were recorded via the digital multimeter (Fig. 1c).

2.5 Evaluation of special functions of the SSSAF

2.5.1 Harvesting of wind energy

The SSSAF with sandwich structure mentioned in section 2.1.3 was a typical polymer based flexible nanogenerator which was used to harvest energy from ambient environments (e.g. human activities, ocean waves, mechanical vibration, wind) via triboelectric or piezoelectric effects [31-34]. Herein, the SSSAF based nanogenerator was used to harvest wind energy by coupling with an energy storage circuit consisting of two diodes and two capacitors (Fig. 1d). The alternating current (AC) voltage generated by the SSSAF based nanogenerator was first half-wave rectified and then stored in two capacitors which could be used in series. Compared with the full wave rectifier, less diodes of our circuit made it more compact and led to less power dissipation. During the wind energy harvesting, the windmill blades were driven by air flow of 5.3 cm/s which was the same flow rate as that in the particle filtration test.

2.5.2 Inhibiting bacteria by the harvested energy

The harvested energy was used to inhibit the growth of bacteria on the SSSAF in the form of electrical discharge. The antibacterial effect was evaluated via the colony counting method using *Bacillus Subtilis* (*B. Subtilis*) as the model bacteria. *B. Subtilis* were cultured in 50 ml liquid Luria Bertani (LB) broth (10 g/L tryptone, 5 g/L yeast extract and 5 g/L sodium chloride) in an incubator at 37 ℃ and 50% RH for 24 hours. Next, the bacteria were separated from the LB liquid broth by centrifuge and prepared as a bacteria-water suspension at the concentration of 1.0×10^7 cell/ml. 200 μL bacteria-water suspension was sprayed on the SSSAF and an electrical discharge at 5V voltage was applied on the filter surface loaded with bacteria at a frequency of 14 times per

hour (Fig. 1e). The electrical discharge was performed by the capacitors charged by the SSSAF based nanogenerator. After electrical discharge treatment, the PZT/PVDF membrane inside the SSSAF was taken out and eluted with 10 ml water, then 100 μL eluent was spread on the prepared LB agar plates (15 g/L agar, 10 g/L tryptone, 5 g/L yeast extract and 5 g/L sodium chloride) and cultured in the incubator at 37 ℃ and 50% RH for 24 hours. The number of *B. Subtilis* bacteria colonies were counted and compared with the control sample. The SSSAF, water, and broth were sterilized before use.

3. Results and discussion

3.1 Piezoelectric property of the SSSAF

Compared with the peak output voltage (~ 6 V) of the SSSAF equipped with pure PVDF membrane, the peak output voltage of the SSSAF equipped with PZT/PVDF membrane was enhanced and influenced by the PZT concentration (Fig. 2a). First, the dielectric constant of PZT/PVDF membrane was enhanced by the addition of PZT powder [35], leading to the increase of the peak output voltage. Secondly, the fraction of PZT in the fibers increased with increasing PZT concentration, which led to the fibers with bigger diameters (Fig. 2b). Due to the higher mass, the bigger fibers generated less vibration in response to external mechanical vibration, and finally resulted in the lower output voltage at high PZT concentration. The positive effect of PZT on piezoelectric property was predominant when the PZT concentration was less than 1%, whereas the negative effect of PZT was more obvious when the PZT concentration increased to 2% (Fig. 2a and Fig. 2b).

The higher fraction of β crystal phase in PVDF may be another reason for 1% being the optimal PZT concentration in PZT/PVDF membrane. As shown in Fig. 2c, with the

addition of PZT powder, the intensity of PZT characteristic peaks increased, while the intensity of PVDF characteristic peak was lower compared to pure PVDF. Among the PZT/PVDF membranes loaded with different PZT concentrations, the PZT/PVDF membrane with a PZT concentration of 1% demonstrated the maximum intensity of the characteristic peak at $2\theta = \sim 20°$, which indicated high fraction of β crystal phase of PVDF molecules. PZT can serve as a source of electric field during polarization and promote the transformation of other polymer phases into β crystal phase [36]. On the other hand, finer electrospun PVDF nanofibers show higher β crystal phase [37]. Due to the above two competing effects, the highest fraction of β crystal phase in PZT/PVDF fibers occurred at finite PZT concentration which was found to be around 1% in the present study.

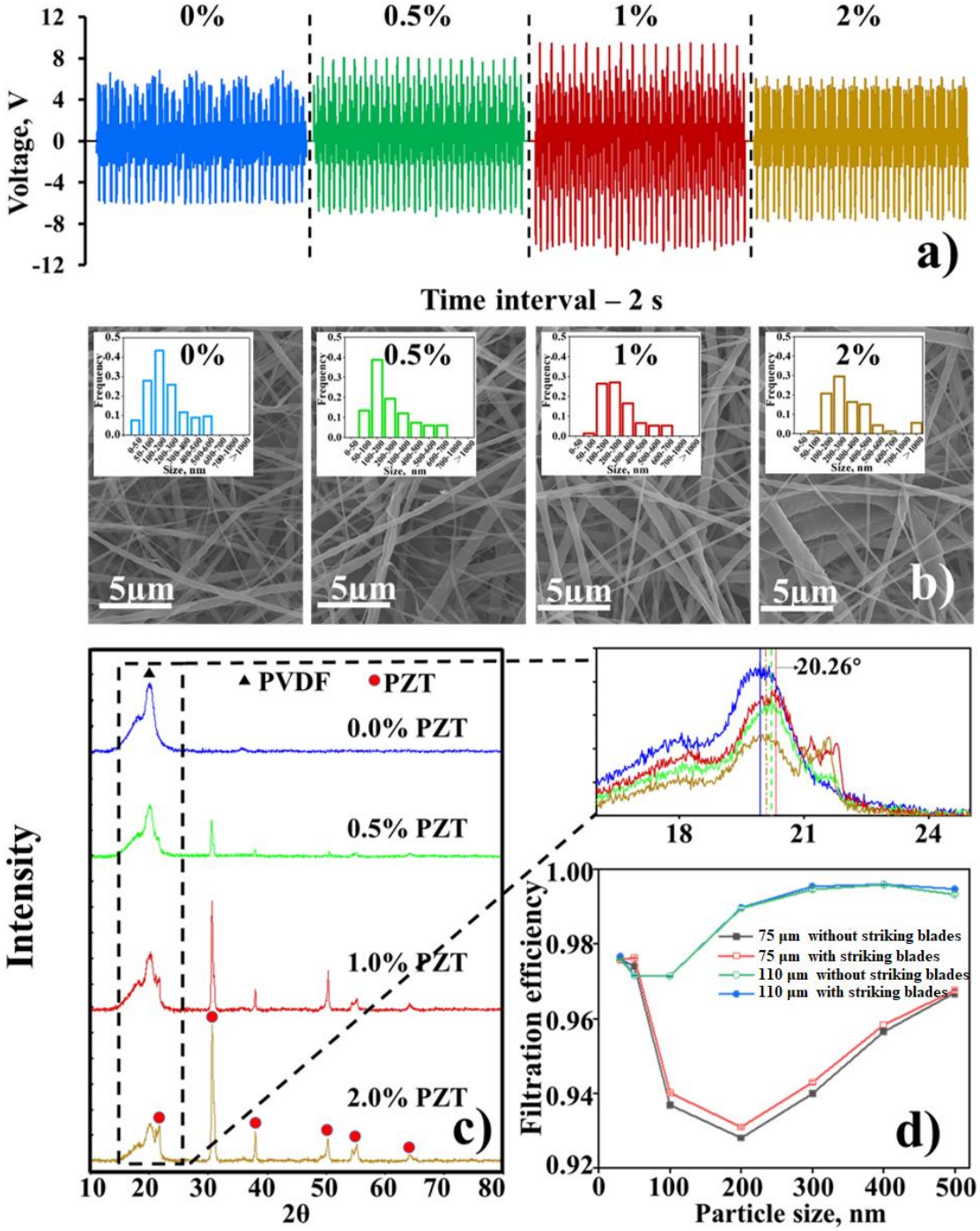

Fig. 2. a) Output voltage of the SSSAF equipped with different PZT/PVDF membranes. b) SEM images of PZT/PVDF membranes with different PZT concentrations, and the diameter distributions of PZT/PVDF fibers. c) XRD patterns of PZT/PVDF membranes with different PZT concentrations. d) Particle filtration efficiencies of the SSSAF equipped with PZT/PVDF membranes of different thicknesses (75 and 110 μm) with and without the striking blades.

The piezoelectric performance of the SSSAF was also affected by the area and thickness of the PZT/PVDF membrane. For the PZT/PVDF membranes with the same thickness of 110 μm, the peak output voltage increased from ~ 3 to ~ 12 V with the membrane area increased from 11 to 100 cm^2 (Fig. S2a). With the PZT/PVDF membrane area of 66 cm^2, the peak output voltages with thicknesses of 62.5, 75 and 110 μm were ~ 4, ~ 6 and ~ 10 V, respectively (Fig. S2b). In addition, several materials commonly used as filtration media were selected as reference samples to prove the voltage signal was generated due to the specific properties of the PZT/PVDF membrane. The results showed that the piezoelectric voltage signals of paper filter, PTFE membrane and nylon membrane were negligible compared with the PZT/PVDF membrane (Fig. S2c). In the following experiments, the SSSAF was equipped with the PZT/PVDF membrane with PZT concentration of 1%, area of 100 cm^2 and thickness of 110 μm.

3.2 Filtration efficiency of the SSSAF

As shown in Fig. 2d, the SSSAFs equipped with thicker PZT/PVDF membrane possessed higher filtration efficiency and smaller most penetrating particle size (MPPS). Similar influences of the filter thickness on filtration efficiency and MPPS were observed in previous works [38,39]. Huang et al. [39] attributed the enhancement of filtration efficiency to the increased particles deposition sites in the thicker filter. Compared with the thinner membrane, the extra thickness of the thicker PZT/PVDF could be considered as an additional electret filter. It is well known that the electret filters can have small MPPS well below 100 nm [40]. Moreover, the extra filter increases the filtration efficiency. Overall, the filtration efficiencies of SSSAFs were higher than 97% for particles below 100 nm, and > 99% for particles over 200 nm. According to the results of filtration test, the windmill blades had no statistically significant effects on the filtration efficiency of the SSSAF.

3.3 Performance of the SSSAF on pressure drop and VOCs sensing

3.3.1 Pressure drop sensing

The pressure drop and the piezoelectric signal of the SSSAF, both affected by the loaded particles, could be correlated. As shown in Fig. 3a, the output peak voltage decreased from ~ 5 to ~ 3 V with the pressure drop of the SSSAF increased by 200 Pa. Within the pressure drop changing (ΔP) range of 0-500 Pa, ΔP and the output peak voltage were linearly related (Fig. 3b). Because of the good response to pressure drop, the SSSAF provides information for when to clean or replace the filter without the need of the differential pressure meter.

There are two possible mechanisms to explain the effects of the loaded particles on the piezoelectric signal. a) The loaded particles acted as a mechanical vibration absorber to reduce the vibration reaching the PZT/PVDF membrane and weaken the piezoelectric signal. b) It is well known that elastic, piezoelectric and dielectric losses are the loss origins in piezoelectrics [41,42]. The loaded particles probably affected the elastic constants, piezoelectric coefficient and dielectric constant of the PZT/PVDF membrane to increase the piezo loss.

3.3.2 VOCs sensing

The resistance of the VOCs sensor fabricated on the SSSAF increased by ~ 1.6 kΩ when exposed to saturated ethanol vapor and the sensor was stable and reversible (Fig. 3c). The ΔR value increased with the increasing of ethanol concentration in the range of 50 to 200 ppm, and it demonstrated a non-linear response toward the ethanol concentration (Fig. 3d). In a previous work about polymer-based resistive VOCs sensor [43], the response time of ~ 30 s and recovery time of ~ 200 s were achieved when chloroform was used to challenge the sensor. Here, we observed the response time of

the sensor was ~ 40 s for ethanol gas and the sensor fully recovered as the ΔR value returned to the baseline within ~ 550 s after flushing the test chamber with dry nitrogen (Fig. 3e).

The absorption of ethanol vapor swelled the PZT/PVDF fiber and further produced cracks in the VOCs sensing element (the gold particle layer) on the PZT/PVDF membrane. Cracks created discontinuities in the gold particle layer, which caused increase of the resistance value. The response to the ethanol concentration depended on the swelling degree of PZT/PVDF membrane and the affinity of the PZT/PVDF fibers towards ethanol. Cracks healed after ethanol evaporated, thereby restoring the conductivity of the sensing element. In our previous work [44], different swelling effects were observed when polymer fibers were exposed to different organic compounds, which demonstrated the possibility to achieve the selectivity of the polymer based sensors for various VOCs.

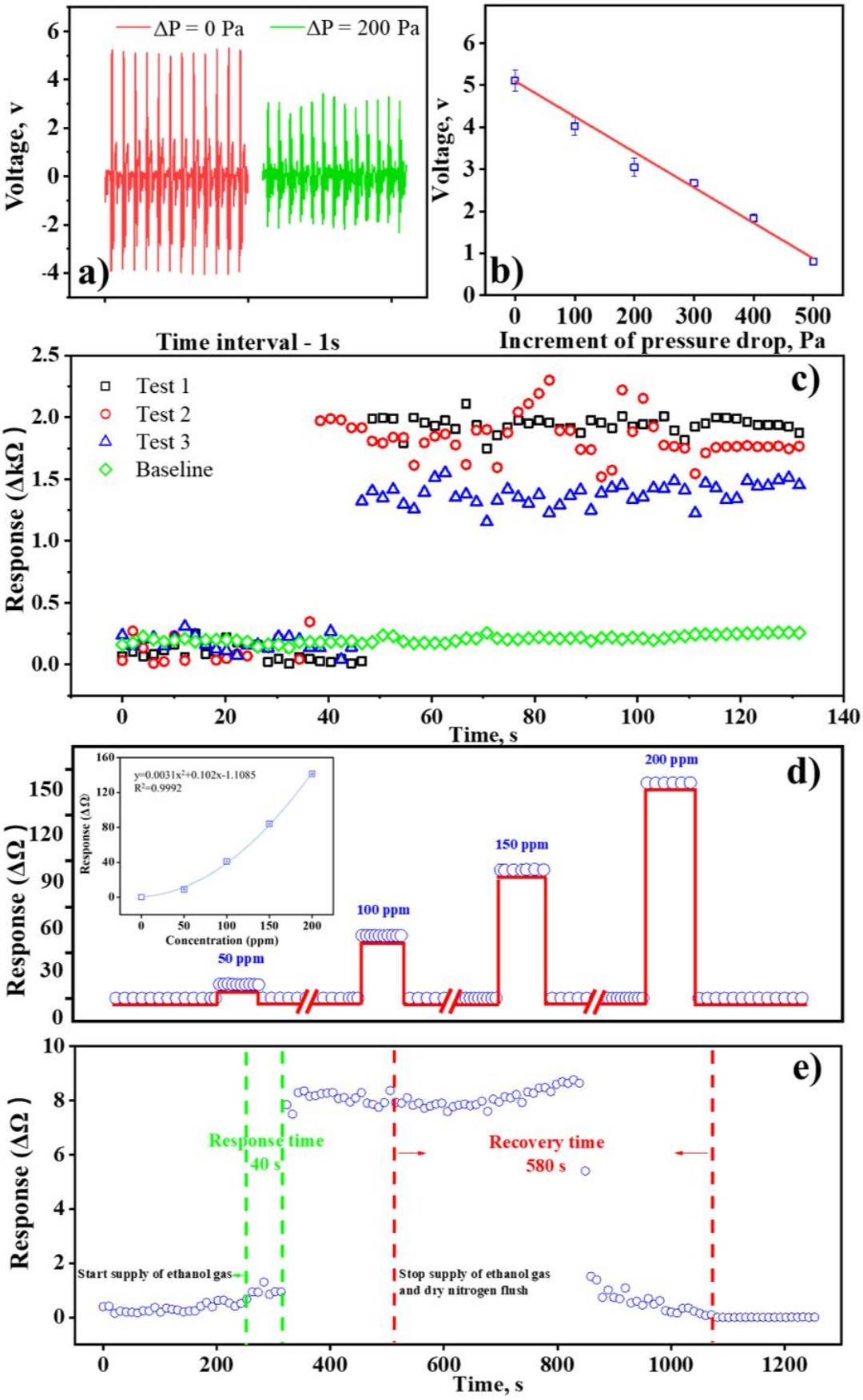

Fig. 3. Pressure drop and VOC sensing functions of the SSSAF. a) Peak voltage of

output signal of the SSSAF when its pressure drop increased from 0 Pa to 200 Pa. b) Output voltage vs. pressure drop relation of the SSSAF. c) The response of the sensor when the SSSAF was exposed to saturated ethanol. d) The response of the sensor at different ethanol concentrations. e) The response time and recovery time of the sensor with an ethanol concentration of 50 ppm.

3.4 Special functions of the SSSAF

3.4.1 Energy harvesting

Three AC voltage signals generated by the SSSAF (Fig. S3), with the peak voltage values (V_{max}) of ~ 6, 7, 8 V, were used for capacitor charging. The capacitors were charged at the fastest speed at the beginning, then the charging speed slowed down, eventually reaching the saturation voltages of ~2.8, 3.2 and 4.0 V, respectively (Fig. 4a). The saturation voltages (V_S) of the capacitors were ~ 50 % of the V_{max} of pulsed AC signal generated by the SSSAF based nanogenerator. V_S depends on the energy transfer efficiency of the energy storage unit. It is well known that the rectifier used in energy storage unit consists of diodes which has a forward voltage (V_F). The diodes were at "off" state when the voltage supplied by the nanogenerator was lower than V_F, which induced the loss of energy and thus the smaller V_S than V_{max} [45]. Zi et al. [46] proposed a plot of built-up voltage V against the transferred charges Q to analyze the charging process of triboelectric nanogenerator for battery/capacitor, and provided an equation to calculate the V_S:

$$V_S = \frac{V_{max}\, V'_{max}}{V_{max}+V'_{max}} \quad (1)$$

where V_{max} is the maximum open-circuit voltage at Q=0, and V'_{max} is the maximum achievable absolute voltage when Q is equal to the maximum short-circuit transferred charge. In the present study, the SSSAF based nanogenerator is similar to the typical

contact-mode freestanding triboelectric-layer-based nanogenerators (CFTENGs) with dielectric-freestanding-layer [47]. $V_{max} = V'_{max}$ because the capacitance between the electrodes is constant [47,48]. According to Equation (1), the saturation voltage of the capacitor can be charged to 50% of V_{max}, which is consistent with the results observed in this study.

In Niu et al. [49], the charging performance of the nanogenerator with a rectifier was proved to be completely analogous to that of a DC voltage source and its charging behavior depended on the load capacitor. Herein, two capacitors with 10 μF and 1000 μF were separately charged by signal 3 (Fig. S3) which had a peak voltage of 8 V, and the charging curves of two capacitors were compared. The results indicated that the two capacitors finally reached almost the same saturation voltage, and it took longer time for the bigger capacitor to reach the saturation voltage (Fig. S4a and Fig. S4b). In addition, the charged 1000 μF capacitor could sustain the LED light for about 30 seconds while the 10 μF capacitor could only flash the LED once. The result was as expected since the bigger capacitor stored more energy than the smaller one when both were charged to the same voltage.

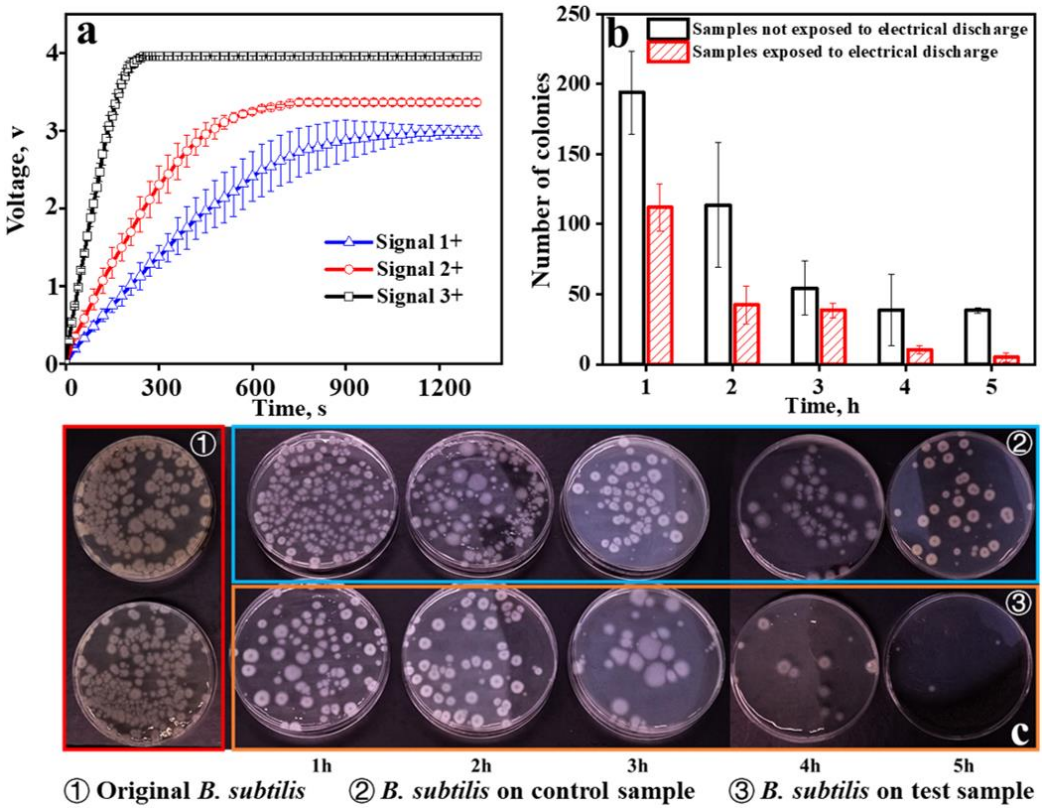

Fig. 4. Test results for the special functions of the SSSAF. a) Charging curves of 10 μF capacitor by the different levels of power generated by the SSSAF based nanogenerator (signal + represents the positive half cycle of the AC signals). b) Bacteria inhibiting effect of the electrical discharge generated by harvested energy. c) Petri dishes for counting of bacteria-formed colonies.

3.4.2 Antibacterial function of the SSSAF

The electrical discharge voltage of 5 V, supplied by the SSSAF charged 10 μF capacitors, was applied on the bacteria contaminated surface of SSSAF for inhibiting the growth of bacteria. Because the 10 μF capacitors could be charged to the saturated voltage of 5 V in ~ 250 s (Fig. 4a), the frequency of the applied electrical discharge was 14 times per hour. As shown in Fig. 4b, the numbers of viable bacteria on both the control sample and test sample decreased over time. When the electrical discharge was applied to *B. subtilis* on the test sample for 5 hours, the number of the survived bacteria

was 4.46% of the original bacteria number. In contrast, the number of viable bacteria on the control sample was ten times of that on the test sample. The effect of the electrical discharge on the number of viable bacteria was clearly visible in the cultured agar plates (Fig. 4c).

Using electric fields for disinfection purposes has been studied for several decades. The most well-known and best understood method was pulsed voltages of 20 kV/cm or higher [50,51]. Actually, the direct electric current of low amperage has been proved to effectively inhibit the growth of several bacteria such as *Staphylococcus aureus*, *Escherichia coli* and *Proteus mirabilis* [52-54]. Until now, the antibacterial mechanism of direct electric current can only be speculated that it disrupts the physiological functions of the microorganisms like the membrane transport [52]. Therefore, it was concluded that the harvested energy functioned via the discharged current to inhibit the growth of *B. subtilis*. In Birbir et al. [54], 100% of extremely halophilic bacteria were killed under the challenge of 0.5 A constant electric current (with 4 V voltage) in 10 minutes. By contrast, a killing rate of 78.02% for *B. subtilis* was achieved in the present study after 70 times of electrical discharge in 5 hours. On the one hand, *B. subtilis* is harder to kill because the endospores produced by *B. subtilis* provided additional protection against environmental stresses [55]. On the other hand, the used electric current in the present work was 700 nA (with 5 V voltage) and gradually decreased during electrical discharge (Fig. S6). The lower current intensity is another reason for the lower killing rate compared to the results of Birbir et al. [54]. However, it should be emphasized that the energy used for inhibiting bacteria in this study was supplied by SSSAF itself; no external power source was needed.

4. Conclusions

In summary, a type of self-supporting smart air filter (SSSAF) based on PZT/PVDF electrospun membrane was developed and multiple features were demonstrated in terms of filtration efficiency, sensing function and two special functions of energy harvesting and bacteria inhibition.

The average filtration efficiency of the SSSAF for particles in the range of 50-500 nm was 98.51%. The SSSAF achieved the pressure drop sensing function by correlating its pressure drop and piezoelectric signal. Thanks to the swelling property of the PZT/PVDF membrane, the SSSAF showed a sensitive response to ethanol gas in the concentration range of 50 to 200 ppm. Such polymer based VOCs sensors are easy to produce with low cost, and they have great potential in various smart systems that require VOCs sensing function. Besides the sensing functions, the SSSAF was used as a nanogenerator to harvest wind energy, and the harvested energy can be effectively used to inhibit the growth of bacteria.

Further work is needed to improve the SSSAF. A better structure design would help to enhance the output power of the SSSAF based nanogenerator. The VOCs sensing property could be improved by employing other polymers or modifying the surface to enhance the affinity between fibers and VOCs. The stimuli-responsive polymers based sensors for monitoring wind velocity, temperature and humidity are expected to be integrated into the SSSAF. Our SSSAF is designed to take advantage of the energy carried by the filtration air flow, which is necessary in any filtration system thus brings a stable and innate energy source. The piezoelectric response and the harvested energy are then used for applications such as assisting sensor functions and bacterial inhibition, thus saving energy and reduce the need for external devices. Overall, this study provides new insight into development of an all-in-one smart air filter to handle the complex contaminants, as well as extending the application of flexible nanogenerator.

Acknowledgements

The work was partially supported by Center for Filtration Research at University of Minnesota. We thank the support of National Science and Technology Major Project of China (Award ID: 2017YFC0211801; 2016YFC0801704; 2016YFC0203701; 2016YFC0801605; 2019JH2/10100004). The authors also thank the financial aid from the project of China Scholarship Council, China.

References

[1] S. Dee, L. Batista, J. Deen, C. Pijoan, Can. J. Vet. Res. 69 (2005) 293-298.

[2] N. A. McLarnon, G. Edwards, J. G. Burrow, Int. J Environ. Health Res. 16 (2006) 313-317.

[3] W. He, Y. Guo, R. Shen, Q. Liu, J. Liu, 342 (2019) 321-327.

[4] C. B. Han, T. Jiang, C. Zhang, X. Li, C. Zhang, X. Cao, Z. L. Wang, ACS nano 9 (2015) 12552-12561.

[5] G. Q. Gu, C. B. Han, C. X. Lu, C. He, T. Jiang, Z. L. Gao, Z. L. Wang, ACS nano 11 (2017) 6211-6217.

[6] C. X. Li, S. Y. Kuang, Y. H. Chen, Z. L. Wang, C. Li, G. Zhu, ACS Appl. Mater. Interfaces 10 (2018) 24332-24338.

[7] J. Chang, L. Zhang, P. Wang, Environ. Sci.: Nano 5 (2018) 811-836.

[8] R. Schluter, U.S. Patent Application No. 12/456,402, Dec. 2010.

[9] P. A. Labadie, U.S. Patent No. 4,786,293, 22 Nov. 1988.

[10] L. M. Pillion, M. E. Smith, U.S. Patent No. 6,315,821. 13 Nov. 2001.

[11] A. Nicosia, W. Gieparda, J. Foksowicz-Flaczyk, J. Walentowska, D. Wesołek, B. Vazquez, F. Prodi, F. Belosi, Sep. Purif. Technol. 154 (2015) 154-160.

[12] Z. Wang, Z. Pan, J. Wang, R. Zhao, J. Nanomater. (2016) 6272983.

[13] C. N. Davies, Air Filtration, Academic Press, London, 1976.

[14] W. C. Hinds, Aerosol Technology, John Wiley & Sons, New York, 1982.

[15] R. C. Brown, Air Filtration, Pergamon Press, Oxford, 1988.

[16] K. Kosmider, J. Scott, Filtr. Separat. 39 (2002) 20-22.

[17] J. Liu, T. Jiang, X. Li, Z. L. Wang, Nanotechnology 30 (2019) 292001.

[18] G. Liu, J. Nie, C. Han, T. Jiang, Z. Yang, Y. Pang, L. Xu, T. Guo, T. Bu, C. Zhang, Z. L. Wang, ACS Appl. Mater. Interfaces 10 (2018) 7126-7133.

[19] C. He, Z. L. Wang, Prog. Nat. Sci-Mater, 28 (2018) 99-112.

[20] P. Michalakos, R. Tom, K. Arnold, U.S. Patent No. 6,503,462. Jan. 2003.

[21] W. Tang, T. H. Kuehn, M. F. Simcik, J. Occup. Environ. Hyg. 12 (2015) 525-537.

[22] M. Osaki, A. Kanagawa, Nucl. Technol. 85 (1989) 274-284.

[23] J. J. Li, Y. N. Zhou, Z. H. Luo, ACS appl. Mater. Interfaces 7 (2015) 19643-19650.

[24] S. W. Hong, D. Y. Kim, J. U. Lee, W. H. Jo, Macromolecules 42 (2009) 2756-2761.

[25] A. V. Shirinov, W. K. Schomburg, Sensor. Actuat. A-Phys. 142 (2008) 48-55.

[26] R. Maus, A. Goppelsröder, H. Umhauer, Atmos. Environ. 35 (2001) 105-113.

[27] A. Cooper, R. Oldinski, H. Ma, J. D. Bryers, M. Zhang, Carbohyd. Polym. 92 (2013) 254-259.

[28] Y. S. Ko, Y. H. Joe, M. Seo, K. Lim, J. Hwang, K. Woo, J. Mater. Chem. B 2 (2014) 6714-6722.

[29] Z. Zhong, Z. Xu, T. Sheng, J. Yao, W. Xing, Y. Wang, ACS Appl. Mater. Interfaces 7 (2015) 21538-21544.

[30] Z. Sun, Y, Yue, W. He, F. Jiang, C. H. Lin, D. Y. Pui, Y. Liang, J. Wang, Build. Environ. (2020) https://doi.org/10.1016/j.buildenv.2020.107020.

[31] F. R. Fan, Z. Q. Tian, Z. L. Wang, Nano energy 1 (2012) 328-334.

[32] F. R. Fan, L. Lin, G. Zhu, W. Wu, R. Zhang, Z. L. Wang, Nano lett. 12 (2012) 3109-3114.

[33] J. Chang, M. Dommer, C. Chang, L. Lin, Nano energy, 1 (2012) 356-371.

[34] X. Wang, Nano Energy 1 (2012) 13-24.

[35] A. K. Zak, W. C. Gan, W. H. A. Majid, M. Darroudi, T. S. Velayutham, Ceram. Int. 37 (2011) 1653-1660.

[36] T. Greeshma, R. Balaji, S. Jayakumar, Ferroelectrics Lett. 40 (2013) 41-55.

[37] H. Shao, J. Fang, H. Wang, T. Lin, RSC Adv. 5 (2015) 14345-14350.

[38] W. W. F. Leung, C. H. Hung, P. T. Yuen, Sep. Purif. Technol. 71 (2010) 30-37.

[39] S. H. Huang, C. W. Chen, Y. M. Kuo, C. Y. Lai, R. McKay, C. C. Chen, Aerosol Air Qual. Res. 13 (2013) 162-171.

[40] D. Q. Chang, S. C. Chen, A. R. Fox, A. S. Viner, D. Y. Pui, Aerosol Sci. Tech. 49 (2015) 966-976.

[41] Y. Chen, Y. Wen, P. Li, International Conference on Information Acquisition, 2004. Proceedings, https://doi.org/10.1109/ICIA.2004.1373354.

[42] A. V. Mezheritsky, IEEE T. Ultrason. Ferr. 51 (2004) 695-707.

[43]E. K. W. Tan, G. Rughoobur, J. Rubio-Lara, N. Tiwale, Z. Xiao, C. A. B. Davidson, C. R. Lowe, L. G. Occhipinti, Sci. Rep. 8 (2018) 13865.

[44] P. Sachinidou, C. Heuschling, J. Schaniel, J. Wang, Polymer 145 (2018) 447-453.

[45] Y. Zi, J. Wang, S. Wang, S. Li, Z. Wen, H. Guo, Z. L. Wang, Nat. Commun. 7 (2016) 1-8.

[46] Y. Zi, S. Niu, J. Wang, Z. Wen, W. Tang, Z. L. Wang, Nat. Commun. 6 (2015) 1-8.

[47] S. Niu, Y. Liu, X. Chen, S. Wang, Y. S. Zhou, L. Lin, Y. Xie, Z. L. Wang, Nano Energy 12 (2015) 760-774.

[48] S. Wang, Y. Xie, S. Niu, L. Lin, Z. L. Wang, Adv. Mater. 26 (2014) 2818-2824.

[49] S. Niu, Y. Liu, Y. S. Zhou, S. Wang, L. Lin, Z. L. Wang, IEEE T. Electron Dev. 62 (2014) 641-647.

[50] A. Mizuno, Y. Hori, IEEE T. Ind. Appl. 24 (1988) 387-393.

[51] A. J. H. Sale, W. A. Hamilton, BBA-Gen. Subjects 148 (1967) 781-788.

[52] W. K. Liu, S. E. Tebbs, P. O. Byrne, T. S. Elliott, J. Infection 27 (1993) 261-269.

[53] X. G. Li, H. B. Cao, J. C. Wu, K. T. Yu, Biotechnol. Lett. 23 (2001) 705-709.

[54] Y. Birbir, M. Birbir, J. Electrostat. 64 (2006) 791-795.

[55] A. Mai-Prochnow, M. Clauson, J. Hong, A. B. Murphy, Sci. Rep-UK 6 (2016) 38610.